Inorganic Chemistry

Article

pubs.acs.org/IC

Interaction between a Transition-Metal Fluoride and a Transition-Metal Hydride: Water-Mediated Hydrofluoric Acid Evolution Following Fluoride Solvation

Michele R. Chierotti,[†,‡] Andrea Rossin,[§] Roberto Gobetto,*[,†,§] and Maurizio Peruzzini*[,§]

[†]Dipartimento di Chimica, Università di Torino, Via Giuria 7, 10125 Torino, Italy

[‡]NIS Centre of Excellence, Via Quarello 11, 10135 Torino, Italy

[§]Consiglio Nazionale delle Ricerche, Istituto di Chimica dei Composti Organometallici (ICCOM-CNR), Via Madonna del Piano 10, Sesto Fiorentino, 50019 Florence, Italy

Supporting Information

ABSTRACT: The reaction between the nickel(II) PCP pincer fluoride complex ($^{t\mathrm{Bu}}$PCP)Ni(F) [$^{t\mathrm{Bu}}$PCP = 2,6-$C_6H_3(CH_2P^tBu_2)_2$] and the tungsten(II) carbonyl hydride CpW(H)$(CO)_3$ (Cp = η^5-$C_5H_5^-$) leads to hydrofluoric acid evolution and formation of the bimetallic isocarbonylic species [CpW$(CO)_2$(μ-κ,C:κ,O-CO)···Ni($^{t\mathrm{Bu}}$PCP)]. The process has been monitored through multinuclear (^{19}F, ^{31}P{^{1}H}, ^{1}H) variable-temperature NMR spectroscopy, collecting ^{19}F T_1 data values for a fluoride ligand bound to a transition metal. The extremely short relaxation time (minimum value of 13 ms at 193 K) is ascribed to the large chemical shift anisotropy of the Ni−F bond (688 ppm). The in-depth NMR analysis has revealed that the fluoride−hydride interaction is not direct but water-mediated, at odds with what was previously observed for the "hydride−hydride" case ($^{t\mathrm{Bu}}$PCP)Ni(H)/CpW(H)$(CO)_3$. Kinetic measurements have unveiled that the first step of the overall mechanism is thought to be solvation of the fluoride ligand (as a result of Ni−F···H_2O hydrogen bonding), while further reaction of the solvated fluoride with CpW(H)$(CO)_3$ is extremely slow and competes with the side reaction of fluoride replacement by a water molecule on the nickel center to form the [($^{t\mathrm{Bu}}$PCP)Ni(H_2O)]$^+$ *aquo* species. Finally, density functional theory analysis of the solvation process through a discrete + continuum model has been accomplished, at the M06//6-31+G(d,p) level of theory, to support the mechanistic hypothesis.

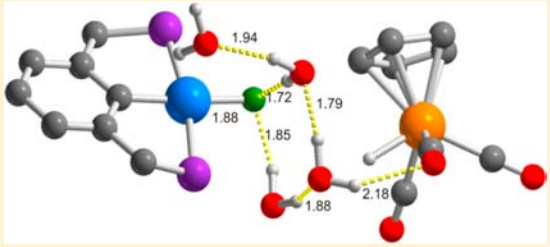

INTRODUCTION

Hydrogen bonding involving fluoride groups is one of the strongest directional, intermolecular, and noncovalent interactions existing in chemistry.[1] The excellent ability of the fluoride ligand of forming hydrogen bonds with proton donors has been extensively documented in the inorganic chemistry literature,[2] where chemical evidence shows that fluorides can act as hydrogen-bonding acceptors in M−$F^{\delta-}$···$^{\delta+}$HA interactions, exhibiting Lewis basic character. Indeed, networks of hydrogen bonds are frequently detected in crystallographic studies of high-valent metal fluorides when suitable proton donors such as the ammonium ion or water are present in the crystal lattice.[3] Most of the bi- and tervalent metal cations are able to form *aquo* complexes with water molecules as ligands; at the same time, these complexes contain fluorides either forming covalent M−F bonds with the metal center or being present as "independent" fluoride anions (i.e., not coordinated). Examples from the first group are the hydrated fluoride salts $FeF_2·4H_2O$[4] and $CuF_2·2H_2O$[5] or the mixed-metal species $CuZrF_6·4H_2O$,[6] while compounds like $[Cr(H_2O)_6]F_3·3H_2O$[7] belong to the second group. A comparison of the mean O−H···F hydrogen-bonding lengths exhibited by the above classes of fluoride hydrates clearly reveals the following trend: if the donor water molecules are engaged in an *aquo* complex, the hydrogen bond is strengthened, but engagement of the acceptor fluorine atoms in a complex anion (like ZrF_6^{2-}) weakens it. A number of structural studies of L_nM−F···H_2O hydrogen bonding (where M = transition metal and L = organic ligand) can be also found in the literature.[8] A special proton donor is hydrofluoric acid (HF): the reaction between HF and L_nM−F often leads to formation of the bifluoride ligand [F−H−F]$^-$ on the metal center. The most common synthetic methodology employed for the preparation of bifluoride complexes is the reaction between the corresponding hydrides or fluorides with $Et_3N·3HF$ ("TREAT HF"). The excess of HF favors M−F···H−F hydrogen-bonding formation. At present, many examples of transition-metal bifluoride complexes are known;[9] structural studies have unveiled the existence of both linear and bent HF_2^- coordination modes to metal ions. In addition, 1D and 3D coordination polymers showing M−F−H−F−M pillars/bridges could also be prepared, using pyrazine as a bridging ancillary ligand.[10]

Received: July 12, 2013
Published: October 14, 2013

   dx.doi.org/10.1021/ic401798b | *Inorg. Chem.* 2013, 52, 12616−12623

Recently, we have reported on the existence of an unconventional M−H$^{\delta-}$···$^{\delta+}$H−M′ dihydrogen bonding between an acidic and a basic transition-metal hydride,[11] along with the isolobal nature of the hydride and fluoride ligands in the pincer-type nickel(II) complexes ($^{t\mathrm{Bu}}$PCP)Ni(H) [**1**; $^{t\mathrm{Bu}}$PCP = 2,6-$C_6H_3(CH_2P^tBu_2)_2$] and ($^{t\mathrm{Bu}}$PCP)Ni(F) (**2**).[12] The replacement of the hydride ligand in **1** with a (more electronegative) fluoride substituent increases the Ni−E (E = H, F) bond polarization considerably. The present study aims at gaining deeper knowledge on the nature of the noncovalent interaction occurring between **2** and the acidic tungsten(II) hydride $CpW(H)(CO)_3$ (**3**; Cp = η^5-$C_5H_5^-$; Scheme 1), under

Scheme 1. Organometallics Studied in This Work

1 2 3

the same experimental conditions as those employed for the "hydride−hydride" case.[11] While "classical" hydrogen bonding between transition-metal fluoride complexes and organic proton donors has already been reported in the literature,[1,2] no examples of metal fluoride−metal hydride interactions have been studied at present (to the best of our knowledge). Multinuclear (^{19}F, ^{31}P{^{1}H}, ^{1}H) variable-temperature (VT) NMR spectroscopy has been exploited as a powerful tool to gain insight into the interaction mechanism.[13] The direct involvement of water in the process leading to HF evolution is confirmed by the spectroscopic data. As a complement, density functional theory (DFT) calculations were performed at the M06//6-31+G(d,p) level on a model system, following the methodology previously employed by some of us for the computational modeling of organometallic proton-transfer reactions in aqueous media.[14]

EXPERIMENTAL SECTION

General Considerations. All reactions were performed using the standard Schlenk procedures under a dry nitrogen atmosphere, unless specified. All solvents employed were purged with nitrogen for 10 min before use. ($^{t\mathrm{Bu}}$PCP)Ni(F) (**2**) was prepared according to the literature procedure,[12] while $CpW(H)(CO)_3$ (**3**; Aldrich) was purified by sublimation before use and stored at −30 °C. Deuterated solvents (Aldrich) were degassed by three freeze−pump−thaw cycles before use.

Multinuclear VT (^{19}F, ^{31}P{^{1}H}, ^{1}H) Solution NMR Spectroscopy. VT ^{19}F, ^{31}P{^{1}H}, and ^{1}H NMR spectra were recorded on a Jeol Eclipse+ 400 MHz spectrometer, equipped with a low-temperature measurement tool. Temperature calibration was carried out with a standard methanol ^{1}H thermometer. Referencing is relative to external tetramethylsilane (^{1}H and ^{13}C), 85% H_3PO_4 (^{31}P), and CCl_3F (^{19}F). 2D ^{1}H NOESY and ^{19}F−^{1}H HOESY spectra were recorded on a Bruker DRX 400 MHz spectrometer with a mixing time of 800 and 75 ms, respectively.

Nonselective inversion recovery was used to obtain ^{1}H T_1 values. Errors in the reported T_1 values were estimated to be in the range ±2%.

Sample Preparation. A tetrahydrofuran (THF)-d_8 solution of **2** (1.5 equiv) prepared in a Schlenk flask kept at 273 K (ice bath) was transferred via cannula into a 5 mm screwed-cap NMR tube containing a THF-d_8 solution of **3** stored at 195 K (dry ice/acetone bath). The samples were degassed using standard freeze−pump−thaw techniques, then transferred into the NMR spectrometer (kept at 190 K), and warmed stepwise to room temperature.

Solid-State NMR Measurements. The solid-state magic-angle-spinning (MAS) ^{19}F NMR spectrum of **2** was recorded on a Bruker 400 Avance II operating at 376.59 MHz for ^{19}F. A cylindrical 2.5-mm-o.d. zirconia rotor with a sample volume of 12 mL was employed and spun at 28 kHz at room temperature. A direct excitation experiment was used with a ^{19}F 90° pulse of 5.35 μs and a relaxation delay of 1 s for 512 scans. The ^{19}F scale was referenced with the resonance of external solid poly(tetrafluoroethylene) (Teflon).

Kinetic Measurements. Variation of the concentration of **2** during the reaction with **3** was monitored at 273 K through integration of the related ^{31}P{^{1}H} NMR signal, both in pure THF (freshly distilled from sodium benzophenone under nitrogen) and in THF/water binary mixtures at different water molarities ranging between 0.1 and 1.3 M (corresponding to relative 1:1:1 and 1:1:20 **2**/**3**/H_2O stoichiometric ratios, respectively). A coaxial external standard of a toluene-d_8/triphenylphospine oxide solution (0.23 M, δ_P = 27.7 ppm, singlet) was employed to have a reference signal for the peak integration. ^{31}P{^{1}H} NMR spectra were recorded on a Bruker Avance II 300 MHz spectrometer; ^{31}P{^{1}H} was referenced to 85% H_3PO_4 with the downfield shift taken as positive.

Computational Details. DFT calculations were performed using the *Gaussian09* program (revision A.02).[15] Model structures were optimized with a M06 functional[16] (already employed successfully in other cases for the treatment of noncovalent bonds[17]) using the SDD (Ni, W)[18]/D95 (P)[19] pseudopotentials and related basis sets on the nickel, tungsten, and phosphorus atoms, a 6-31G* basis on carbon, oxygen, and the pincer protons, and a more extended 6-31+G(d,p) basis on the fluoride−hydride ligands and the water protons. The introduction of diffuse functions is essential to well-reproduce conformational equilibria and experimental electron affinities.[20] An extra d-type polarization function for phosphorus and an extra f-type function for nickel and tungsten were added to the standard set.[21] Gibbs energy calculations to infer relative thermodynamic stabilities were carried out on a *model* system, with the *tert*-butyl groups on the pincer ligand replaced by hydrogen atoms ($^{\mathrm{H}}$PCP). The model compound ($^{\mathrm{H}}$PCP)Ni(F) (**2**$^{\mathrm{H}}$) was therefore used in the simulations. A *discrete-continuum* modeling of the reaction medium was employed. A cluster made of four water molecules $(H_2O)_4$ was explicitly included in the model, and the internal energies were evaluated in a water/THF solution, where the molar fraction of water was assumed to be 0.1 (approximately corresponding to a 1.3 M concentration), represented as a polarizable continuum medium (SMD, ε = 10.09)[22,23] with the same basis set used for the gas-phase optimizations, following the methodology recently employed by some of us for DFT studies of organometallic hydride reactivity in aqueous solutions. This cluster size was previously found to be the optimal compromise between a realistic system description and reasonably short computational times.[14,24] Gibbs energy in solution was calculated according to the simplified equation:

$$G_{solv} = G_{gas} + (E_{solv} - E_{gas})$$

For the transition state TS_1, analytical frequencies were calculated to check that only one imaginary value is obtained, related to a saddle point on the potential energy surface (PES). Normal-coordinate analyses on these stationary points were also performed by intrinsic reaction coordinate (IRC) calculations[25] in both directions to the correspondent minima. When the IRC calculations failed to reach the minima, geometry optimizations from the initial phase of the IRC path were performed.

RESULTS AND DISCUSSION

a. Multinuclear VT NMR Experiments. Equimolar amounts of **2** and **3** were mixed in carefully degassed THF-d_8 at 193 K under a nitrogen atmosphere. A slow temperature increase to 298 K led to a dark-orange solution, from which a reddish-orange crystalline material precipitated, with concom-

dx.doi.org/10.1021/ic401798b | Inorg. Chem. 2013, 52, 12616−12623

Scheme 2. Water-Assisted HF Evolution from the 2−3 Interaction

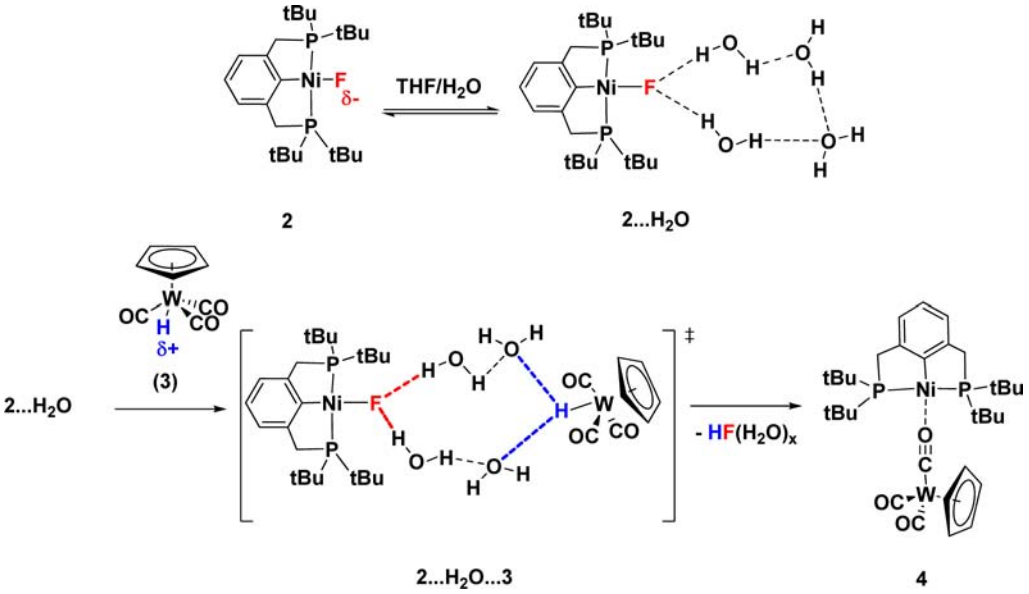

itant HF formation. NMR analysis revealed that the final product is the same as that obtained from the reaction of the analogous hydride compound **1**, the bimetallic compound **4**. Here, we demonstrate that the **2**−**3** interaction, in spite of generating the same final product, takes place through a different mechanism. As IT was already reported, the **1**−**3** reaction implies the formation of a **1**···**3** adduct through an Ni−H···H−W direct interaction.[11] On the contrary, in the case of the fluoride **2**, the reaction seems to proceed through formation of a putative **2**···$\mathbf{H_2O}$···**3** adduct (Scheme 2), as a consequence of the (unavoidable) presence of water coming from the synthesis of **2**.[26]

In order to cast light on the reaction mechanism, a thorough NMR analysis that combines a multinuclear and multiparametric VT approach (^{1}H, ^{19}F, ^{31}P{^{1}H}, ^{1}H NOESY, ^{19}F−^{1}H HOESY, ^{1}H, and ^{19}F T_1 relaxation measurements) was performed. All ^{1}H, ^{19}F, and ^{31}P{^{1}H} NMR chemical shifts (δ) with assignments for reagents, intermediate, and product are listed in Table S1 in the Supporting Information (SI). Table S2 in the SI reports the ^{1}H NMR chemical shifts, together with T_1(^{1}H) relaxation values at different temperatures, while Table S3 in the SI is the same data collection for ^{19}F. The ^{1}H NMR spectrum of pure **3** in THF-d_8 at 293 K (Figure S1 in the SI) is characterized by the Cp and WH resonances at 5.63 and −7.37 ppm, respectively. In both pure **3** and **2**···$\mathbf{H_2O}$···**3**, the hydride resonance at −7.37 ppm slightly shifts toward lower frequencies with decreasing temperature, but both the scalar coupling and line width do not change (Figure S2 and Table S2 in the SI).

No hydride shift is observed upon **2**···$\mathbf{H_2O}$···**3** formation, although a substantial change in the hydride relaxation time occurs (vide infra). This indicates formation of a weak interaction involving the hydride ligand (NOESY and HOESY experiments will clarify the role of water in the interaction; see below). The lack of a signal shift agrees with the limited amount of **2**···$\mathbf{H_2O}$···**3** formed and the small shift of only 0.04 ppm for the direct Ni−H···H−W interaction previously found.[11]

The ^{19}F signal at −372.6 ppm of pure **2** undergoes a significant high-frequency shift (1.5 ppm) when equimolar amounts of **3** are added (Table S3 in the SI). It is also worth noticing that a large increase of the ^{19}F line width was observed for pure **2** (Figure S3 in the SI) and for **2**···$\mathbf{H_2O}$···**3** (Figure 1)

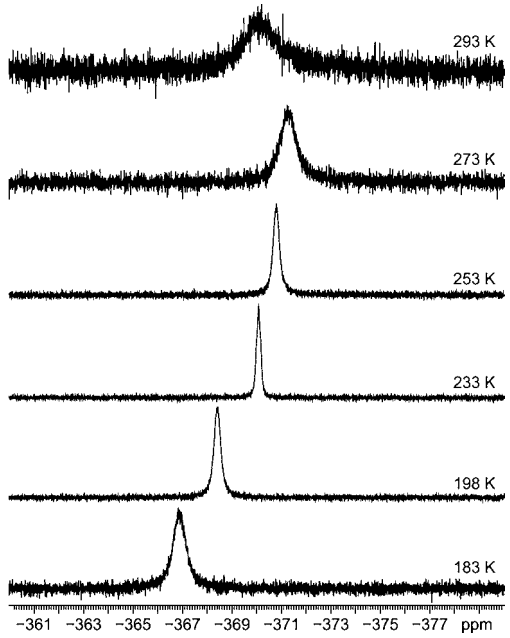

Figure 1. VT ^{19}F (376.59 MHz) NMR spectra (THF-d_8) of **2**···$\mathbf{H_2O}$···**3**.

with decreasing temperature, preventing the direct measurement of the fluorine−hydrogen coupling constants. This behavior is explained in terms of very short ^{19}F T_2 values in agreement with the extremely short T_1 values (see below).

After the solution was left at 263 K for 3−4 h, the doublet assigned to solvated HF [i.e., HF·$(H_2O)_n$] started to appear on both ^{1}H and ^{19}F NMR spectra (^{1}H, 11.64 ppm; ^{19}F, −184.7 ppm; $^1J_{HF}$ = 422 Hz; Figure S4 in the SI), in agreement with the formation of **4** with HF evolution. At odds with other literature cases,[9] no Ni−FHF bifluoride complex formation was observed: only *one sharp* ^{19}F NMR doublet is recorded (Figure S4 in the SI). This can be justified by the very small amount of

dx.doi.org/10.1021/ic401798b | *Inorg. Chem.* 2013, 52, 12616−12623

HF present in solution at all times and temperatures [the reaction leading to **4** and HF is extremely slow, as evidenced by the kinetic studies reported in section c]. Bifluoride complexes normally form from organometallic fluorides under an *excess* of HF.

Informative results came from analysis of both ^{1}H NOESY and ^{19}F−^{1}H HOESY experiments. The ^{1}H NOESY spectrum of **2···H$_2$O···3** collected at 263 K only shows intramolecular NOESY cross peaks (red signals in Figure 2) between the ^{t}Bu

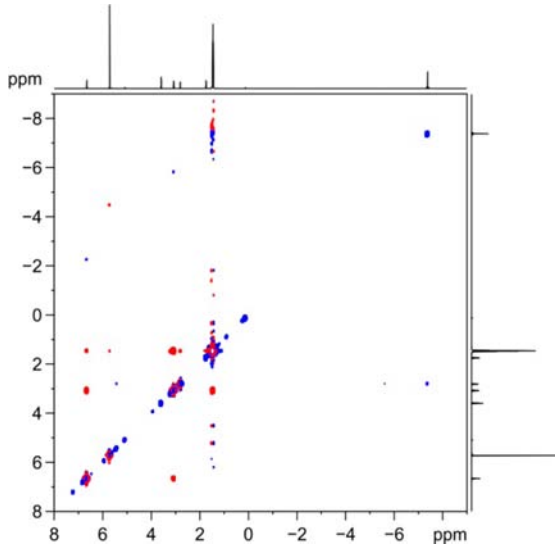

Figure 2. ^{1}H (400.23 MHz) NOESY spectrum (THF-d_8) of **2···H$_2$O···3** recorded at 263 K with a mixing time of 0.8 s. Red negative and blue positive signals represent NOESY and EXSY correlations, respectively.

and Cp protons, in agreement with formation of the adduct as well as with the theoretical calculations (vide infra). Other intramolecular correlations are observed between the CH$_2$/^{t}Bu (3.06/1.43 ppm), phenyl/CH$_2$ (6.64/3.06 ppm), phenyl/^{t}Bu (6.64/1.43 ppm), and hydride/Cp (−7.38/5.71 ppm, not visible in the figure) protons. An exchange process was also found between H$_2$O and the hydride **3** protons (2.80/−7.38 ppm; blue cross peaks in Figure 2). However, no H$_2$O/**3** EXSY cross peaks were observed during recording of the ^{1}H NOESY experiment (even with several mixing times) of pure **3**. The latter finding is in line with the outcome of theoretical analysis (vide infra), which confirms the absence of strong interactions of water with the W−H bond in **3**. From a purely experimental point of view, *aquo* complex formation is not observed in the case of a wet THF solution of pure **3**, with the hydride being rather inert toward water.

Interestingly, the ^{1}H NOESY spectrum of the analogous **1···3** adduct (acquired under the same experimental conditions) did not show any EXSY cross peaks.

This indicates that the reaction mechanism is different and is related to the type of substituent on the nickel center, i.e., hydride or fluoride. In this sense, polarization of the Ni−F bond plays a fundamental role in activating solvation phenomena through the formation of Ni−F···H$_2$O hydrogen bonds, which have a deep influence on the mechanism of the Ni−W interaction. As an additional proof of evidence, the ^{19}F−^{1}H HOESY spectrum collected at T = 243 K (Figure 3) is characterized by the NOESY **2**/H$_2$O cross peak and by the lack of NOESY cross peaks between the fluoride and hydride

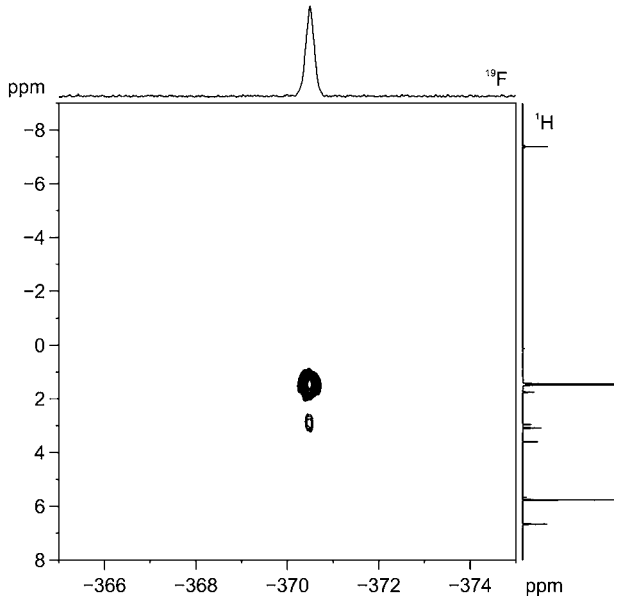

Figure 3. ^{19}F−^{1}H HOESY NMR spectrum (THF-d_8) of **2···H$_2$O···3** recorded at 243 K with a mixing time of 75 ms. NOESY peaks are observed for F/^{t}Bu (−371.4/1.45 ppm) and F/H$_2$O (−371.4/2.95 ppm).

signals. This definitely highlights the water role in assisting and mediating the **2**−**3** interaction.

b. T_1 Relaxation Analysis. ^{19}F T_1 of pure **2** is only 97 ms at 293 K. This value decreases with decreasing temperature, reaching a minimum value of 13 ms between 193 and 183 K and then slowly increasing to 16 ms at 173 K. Elecetron paramagnetic resonance measurements ruled out the presence of paramagnetic impurities responsible for the extremely short T_1 values. At the same time, the small relaxation times cannot be ascribed to the dipolar contribution (which would justify these values only in the presence of very short F···F or F···H interactions; the existence of these contacts is ruled out by the NOESY and HOESY experiments). Moreover, there is no dependence of T_1 from the sample concentration, thus excluding any phenomenon of molecule aggregation in solution. Therefore, the very short ^{19}F T_1 values can be ascribed to the chemical shift anisotropy (CSA) mechanism, according to eq 1:

$$\frac{1}{T_1} = \frac{2}{15}(\sigma_{\parallel} - \sigma_{\perp})^2 \omega_F{}^2 \tau_c \frac{1}{1 + \omega_F{}^2 \tau_c{}^2} \qquad (1)$$

where $\sigma_{\parallel}$ and $\sigma_{\perp}$ refer to parallel and perpendicular shielding with respect to the magnetic field, respectively, τ_c is the correlation time, and ω_F is the fluorine Larmor frequency.

The fast ^{19}F relaxation is triggered by the high gyromagnetic ratio and CSA, although the known literature values for fluorine anisotropy mostly refer to C−F bonds in organic compounds, and therefore they are rather limited.[27] Equation 1 has a minimum when $\omega_F\tau_c$ = 0.62, and then the experimental T_1 value measured at 193 K provides a value for the ^{19}F CSA of about 688 ppm. This value is the largest ever recorded for ^{19}F anisotropy but also the only one, to our knowledge, referring to an M−F interaction, with M being a transition metal. On the other hand, a large CSA value is expected because the ^{19}F chemical shift of **2** (approximately −370 ppm; it represents the isotropic value of the three components of the shielding tensor) is quite far away from the commonly found ^{19}F NMR chemical

dx.doi.org/10.1021/ic401798b | *Inorg. Chem.* 2013, 52, 12616−12623

shift range. Thus, the solid-state MAS ^{19}F NMR spectrum of **2** has been recorded (Figure S4 in the SI). In addition to the isotropic peak, an extended pattern of spinning sidebands associated with a CSA of about 663 ± 20 ppm (span value, following the Herzfeld–Berger convention[28]) can clearly be seen, in good agreement with the anisotropy value calculated in solution. Very short ^{19}F T_1 values preclude the possibility of using the ^{19}F relaxation times to confirm the formation of **2**–$\mathbf{H_2O}$ or **2**–**3** interactions because the contribution of the heteronuclear dipolar mechanism is negligible compared with the much more efficient CSA mechanism. In line with this statement, the ^{19}F T_1 values are almost identical for pure **2** and for **2**···$\mathbf{H_2O}$···**3**. Interestingly, the ^{19}F signal line width increases with decreasing temperature; this is due to the very short T_2 values related to the high CSA contribution to spin–spin relaxation, according to eq 2.

$$\frac{1}{T_2} = \frac{2}{15}(\sigma_{\parallel} - \sigma_{\perp})^2 \omega_F{}^2 \tau_c \left(\frac{2}{3} + \frac{1}{2} \frac{1}{1 + \omega_F{}^2 \tau_c{}^2} \right) \quad (2)$$

Conversely, ^1H T_1 values of the hydride resonance of **3** showed a remarkable decrease when equimolar amounts of **2** were added to the solution, passing (for example) from 7.2 to 5.8 s at 198 K. This suggests that an additional contribution to ^1H T_1 due to dipole–dipole intermolecular interaction with the Ni–F–water cluster may be present, according to eq 3:

$$\frac{1}{T_1} = \frac{3}{10} \left(\frac{\mu_0}{4\pi} \right) \frac{\gamma_H{}^4 \hbar^2}{r_{HH}{}^6} \tau_c \left(\frac{1}{1 + \omega_H{}^2 \tau_c{}^2} + \frac{4}{1 + 4\omega_H{}^2 \tau_c{}^2} \right) \quad (3)$$

γ_H is the ^1H gyromagnetic ratio, h is the Boltzmann constant, r_{HH} is the internuclear H---H distance, and ω_H is the proton Larmor frequency.

c. Kinetic Studies: Formation of the *Aquo* Complex [(^{tBu}PCP)Ni(H_2O)]$^+$ (5). The role of water in the reaction between **2** and **3** evidenced by the NOESY and HOESY NMR spectra has been further analyzed through kinetic measurements of the reaction rate through $^{31}P\{^1H\}$ NMR signal integration in the presence of an external standard. Experiments were performed at 273 K with different THF/water mixtures (water molarities ranging between 0.1 and 1.3 M). While −d[**2**]/dt was monitored in wet THF (1.3 M in H_2O), within the first 13 min (ca. 800 s) a significant decrease of the fluoride concentration was recorded (Figure 4). This is surely related to replacement of the fluoride ligand by an *aquo* ligand on a nickel(II) coordination sphere, with concomitant formation of **5** and the solvated fluoride anion $[F(H_2O)_x]^-$ (as an ion pair).

In line with this hypothesis, a new $^{31}P\{^1H\}$ NMR signal at δ_P 74.4 and growing with time started to appear together with that of **4** (Figure S6 in the SI). This signal had been previously assigned to the cation **5**, by adding water to pure **2** in THF in an independent experiment.[29] From all of these results, it can be stated that water acts as a competitive reagent toward **2**, and the higher its concentration, the slower will be formation of **4**. Evolution to the bimetallic product is severely hampered by the solvation sphere created by water around the F^- ligand. At this stage, the reaction rate becomes extremely slow, and the concentration of **2** is practically constant in time (because its consumption is too slow to be measured accurately in a reasonable time scale; only a negligible statistical deviation of the collected kinetic data points from a mean constant value is recorded; Figure 4). Therefore, it is impossible to propose any meaningful kinetic law for formation of **4**.

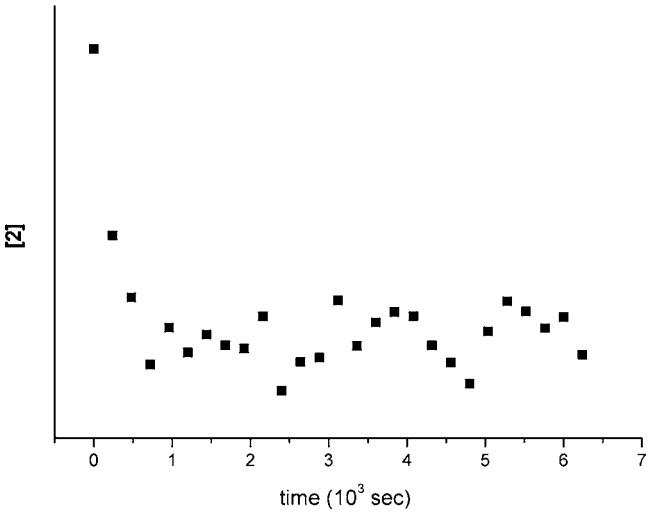

Figure 4. Variation of [**2**] in time in a **2**···$\mathbf{H_2O}$···**3**/wet THF solution {T = 273 K, [H_2O] = 1.3 M, **2**:**3**:H_2O stoichiometric ratio = 1: 1: 20}. The Y-axis values are inferred from the $^{31}P\{^1H\}$ NMR signal integration of the characteristic doublet of **2** with respect to an external triphenylphospine oxide standard at known and constant concentration (see the Experimental Section).

d. DFT Modeling of the Solvation Process. The interaction of water with **2** and **3** has been further analyzed from a computational point of view, at the M06//6-31+G(d,p) level of theory. To this aim, a simplified structure for **2** was taken into account for the calculations, where the bulky *tert*-butyl groups were replaced with hydrogen atoms, to achieve the best compromise between model system accuracy and computational time. The resulting complex $\mathbf{2^H}$ was assumed to be the starting reagent. Initially, the direct interaction between $\mathbf{2^H}$ and **3** has been simulated; at odds with what was found in the "hydride–hydride" Ni–H···H–W case,[11] in the optimized model structure, no Ni–F···H–W hydrogen bonding is found. A preferential Ni–F···H–C(Cp) interaction involving the (more acidic) Cp protons is instead observed [optimized d(Ni–F···H–C) = 1.92 Å, $\mathbf{2^H}$···**3**; Figure S7 in the SI]. The calculated Mulliken charges on the fluoride ligand and on the interacting Cp proton are indeed the highest of the whole system (q_F = −0.5 e; q_H = +0.3 e). At the same time, a weak Ni···H–W interaction is also present [optimized d(Ni···H–W) = 2.47 Å]. Both atoms are electronically neutral (Mulliken charges: q_{Ni} = +0.08 e; q_H = +0.05 e). Therefore, HF evolution must take place through a different type of mechanism (i.e., it must be solvent-mediated), with this hypothesis being perfectly in line with the experimental results.

Before the two reagents were put together in the computation, the interaction of $(H_2O)_4$ with $\mathbf{2^H}$ and **3** was examined separately; while $\mathbf{2^H}$ engages in a double Ni–F··· HOH hydrogen bonding [optimized d(Ni–F···HOH) = 1.72 and 1.80 Å; $\mathbf{2^H}$···$\mathbf{(H_2O)}$; Figure S8 in the SI], **3** does not form any kind of hydrogen bonding through its hydride substituent [shortest d(W–H···OH_2) = 2.52 Å]. A preferential interaction with the *carbonyl ligands and Cp protons* occurs instead [optimized d(C≡O···HOH) = 1.90 and 2.08 Å; shortest contact Cp–H···OH_2 = 2.37 Å; **3**···$\mathbf{(H_2O)}$; Figure S9 in the SI]. In line with NMR analysis, the presence of a very small Mulliken charge on the hydride (calculated q_H = +0.06 e)

dx.doi.org/10.1021/ic401798b | Inorg. Chem. 2013, 52, 12616–12623

makes the interaction of water with the CO or Cp ligands more favored than that with the hydride substituent itself. The weak hydrogen-bonding ability of the W−H bond in **3** toward organic bases (phosphine oxides, amines, and pyridine) had already been pointed out in previous spectroscopic and computational studies.[30]

After this preliminary investigation, $\mathbf{2^H\cdots(H_2O)}$ was combined with the (pre)optimized geometry of **3**, and the ensemble was reoptimized; the resulting $\mathbf{2^H\cdots(H_2O)\cdots3}$ adduct is shown in Figure 5. The water cluster is now bridging the

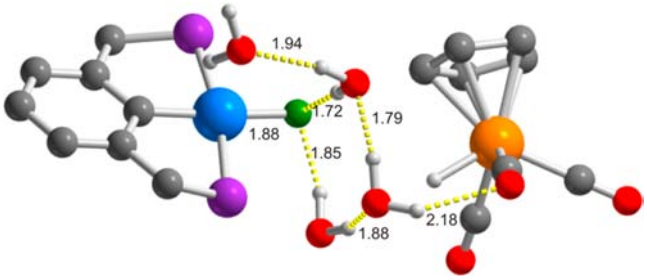

Figure 5. Optimized geometry of $(^{H}PCP)Ni(F)\cdots(H_2O)_4\cdots CpW(H)(CO)_3$ [$\mathbf{2^H\cdots(H_2O)\cdots3}$]. Selected optimized bond lengths are reported (Å). Hydrogen bonds are depicted with yellow dotted lines. Hydrogen atoms on the organic ligands of both complexes are omitted for clarity. Atom color code: white, H; gray, C; purple, P; blue, Ni; orange, W; green, F; red, O.

hydride and fluoride complexes through a complex hydrogen-bonding network. The shortest W−H···OH_2 distance is 2.78 Å, and weak Cp−H···OH_2 and C≡O···HOH interactions are present, as seen in $\mathbf{3\cdots(H_2O)}$ (distances equal to 2.39 and 2.18 Å, respectively).

HF formation is probably induced by an indirect mechanism, where the water bridge acts as a "proton shuttle" between **2** and **3**; this kind of process was also invoked in the case of proton-transfer reactions for water-soluble organometallic hydrides.[14] A PES scan along the d(W−H···OH_2) reaction coordinate was performed; a transition state TS_1 (Figure 6) lying at 9.5 kcal mol^{-1} above the reagent leads to an intermediate structure where the proton coming from W−H bond dissociation is "hosted" by the water cluster: $(^{H}PCP)Ni(F)\cdots(H_2O)_3(H_3O)^+\cdots$

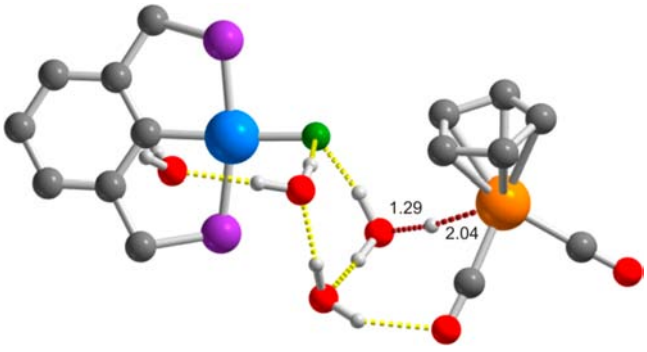

Figure 6. Optimized geometry of TS_1. Selected optimized bond lengths are reported (Å). Bonds directly related to the transition state transformation are drawn with brown dotted lines. Hydrogen bonds are depicted with yellow dotted lines. Hydrogen atoms on the organic ligands of both complexes are omitted for clarity. Atom color code: see Figure 5.

$CpW(CO)_3^-$ ($\mathbf{6^H}$; Figure 7). The ΔG value for the $\mathbf{2^H\cdots(H_2O)\cdots3} \rightarrow \mathbf{6^H}$ transformation equals +5.8 kcal mol^{-1}.

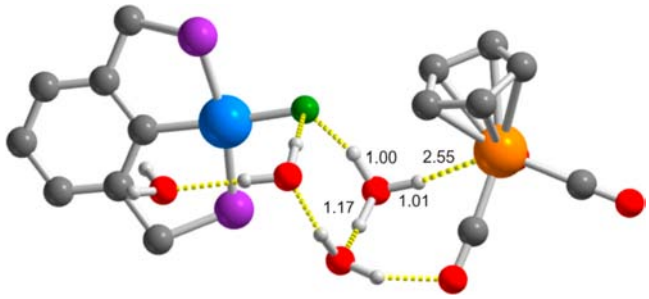

Figure 7. Optimized geometry of $\mathbf{6^H}$. Selected optimized bond lengths are reported (Å). Hydrogen bonds are depicted with yellow dotted lines. Hydrogen atoms on the pincer ligand and Cp ring are omitted for clarity. Atom color code: see Figure 5.

From $\mathbf{6^H}$, fluoride dissociation and concomitant *aquo* complex/HF formation lead to the final structure $[(^{H}PCP)Ni(H_2O)][CpW(CO)_3]\cdots[(HF)(H_2O)_3]$ ($\mathbf{7^H}$; Figure 8). An

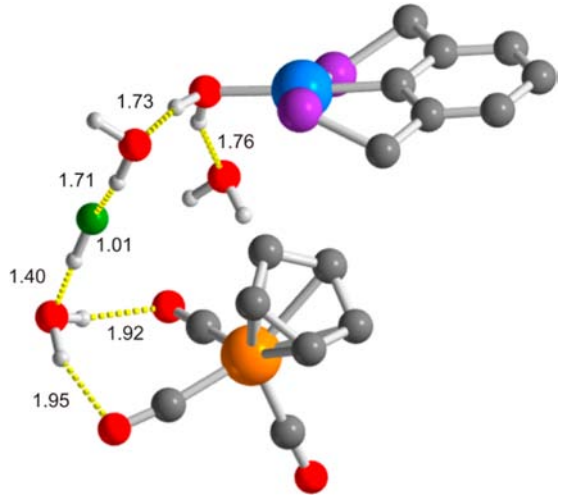

Figure 8. Optimized geometry of $\mathbf{7^H}$. Selected optimized bond lengths are reported (Å). Hydrogen bonds are depicted with yellow dotted lines. Hydrogen atoms on the pincer ligand and Cp ring are omitted for clarity. Atom color code: see Figure 5.

approximate value of the activation barrier for this step is 4.3 kcal mol^{-1}.[31] Thermodynamics is almost thermoneutral for HF formation: the ΔG value for the $\mathbf{2^H\cdots(H_2O)\cdots3} \rightarrow \mathbf{7^H}$ conversion equals −0.5 kcal mol^{-1}. Thus, the higher energy barrier to overcome in order to achieve HF formation under these conditions is around 10 kcal mol^{-1}, small enough for the reaction to occur at ambient temperature.

CONCLUSIONS

The interaction between a transition-metal fluoride and a transition-metal hydride that leads to HF generation has been described; the reaction follows a different mechanistic path with respect to the analogous "hydride−hydride" case. No direct hydride−fluoride reaction takes place; the presence of water is of fundamental importance for the reaction progress, and a water-assisted process may be invoked, through solvation of the fluoride ion followed by a Grotthuss-like proton transfer[32] mediated by a protonated water cluster. Multinuclear VT NMR

dx.doi.org/10.1021/ic401798b | *Inorg. Chem.* 2013, 52, 12616−12623

spectroscopy and DFT simulations on model compounds have been proved to be extremely efficient and complementary tools for accurate analysis of this class of processes.

■ ASSOCIATED CONTENT

Supporting Information

Tables S1−S3, Figures S1−S9, and Cartesian *xyz* coordinates and (selected) absolute G_{solv} energy values of $\mathbf{2^H}$···**3**, $\mathbf{2^H}$···$(\mathbf{H_2O})$, **3**···$(\mathbf{H_2O})$, $\mathbf{2^H}$···$(\mathbf{H_2O})$···**3**, $\mathbf{TS_1}$, $\mathbf{6^H}$, and $\mathbf{7^H}$. This material is available free of charge via the Internet at http://pubs.acs.org.

■ AUTHOR INFORMATION

Corresponding Authors

*E-mail: roberto.gobetto@iccom.cnr.it.

*E-mail: maurizio.peruzzini@iccom.cnr.it.

Notes

The authors declare no competing financial interest.

■ ACKNOWLEDGMENTS

The PIRODE project of the Italian Ministry of the Environment, the EFOR, and "Premiale 2011" projects of the Italian National Research Council are acknowledged for financial support. The use of the computational facilities of the Centre de Serveis Científics i Acadèmics de Catalunya is greatly appreciated. Thanks are also given to the FIRENZE HYDROLAB 2 project supported by ECRF. Fabrizio Zanobini and Andrea Rossi (ICCOM-CNR) are acknowledged for help with the preparation of **2** and for running the kinetic measurements. The authors are indebted to Prof. A. Macchioni and Dr. C. Zuccaccia (University of Perugia, Italy) for use of the NMR facilities in their laboratory and for stimulating discussions.

■ REFERENCES

(1) (a) Steiner, T. *Angew. Chem., Int. Ed.* **2002**, *41*, 48. (b) Brammer, L.; Bruton, E. A.; Sherwood, P. *Cryst. Growth Des.* **2001**, *1*, 277. (c) Desiraju, G. R.; Steiner, T. *The Weak Hydrogen Bond*; Oxford University Press: Oxford, U.K., 1999. (d) Richmond, T. G. *Coord. Chem. Rev.* **1990**, *105*, 221 and references cited therein.

(2) (a) Martinez-Prieto, L. M.; Melero, C.; del Rio, D.; Palma, P.; Campora, J.; Alvarez, E. *Organometallics* **2012**, *31*, 1425. (b) Clot, E.; Eisenstein, O.; Jasim, N.; McGregor, S. A.; McGrady, J. E.; Perutz, R. N. *Acc. Chem. Res.* **2011**, *44*, 333. (c) Dransfield, T. A.; Nazir, R.; Perutz, R. N.; Whitwood, A. C. *J. Fluorine Chem.* **2010**, *131*, 1213. (d) Libri, S.; Jasim, N. A.; Perutz, R. N.; Brammer, L. *J. Am. Chem. Soc.* **2008**, *130*, 7842. (e) Murphy, V. J.; Hascall, T.; Chen, J. Y.; Parkin, G. *J. Am. Chem. Soc.* **1996**, *118*, 7428. (f) Peris, E.; Lee, J. C.; Rambo, J. R.; Eisenstein, O.; Crabtree, R. H. *J. Am. Chem. Soc.* **1995**, *117*, 3485.

(3) Babel, D.; Massa, W. *Chem. Rev.* **1988**, *88*, 275.

(4) Penfold, B. R.; Taylor, M. R. *Acta Crystallogr.* **1960**, *13*, 953.

(5) Prince, E. *J. Chem. Phys.* **1972**, *56*, 4352.

(6) Fischer, J.; Weiss, R. *Acta Crystallogr.* **1973**, *B29*, 1955.

(7) Epple, M.; Massa, W. *Z. Anorg. Allg. Chem.* **1978**, *444*, 47.

(8) (a) Lian, Z.; Xu, X.; Sun, H.; Chen, Y.; Zheng, T.; Li, X. *Dalton Trans.* **2010**, *39*, 9523. (b) Fawcett, J.; Harding, D. A. J.; Hope, E. G.; Singh, K.; Solan, G. A. *Dalton Trans.* **2009**, 6861. (c) Schaub, T.; Fischer, P.; Steffen, A.; Braun, T.; Radius, U.; Mix, A. *J. Am. Chem. Soc.* **2008**, *130*, 9304. (d) Miyamoto, R.; Hamazawa, R. T.; Hirotsu, M.; Nishioka, T.; Kinoshita, I.; Wright, L. J. *Chem. Commun.* **2005**, 4047. (e) Jasim, N. A.; Perutz, R. N.; Whitwood, A. C.; Braun, T.; Izundu, J.; Neumann, B.; Rothfeld, S.; Stammler, H.-G. *Organometallics* **2004**, *23*, 6140.

(9) Pd−FHF: (a) Grushin, V. V. *Acc. Chem. Res.* **2010**, *43*, 160. (b) Ball, N. D.; Sanford, M. S. *J. Am. Chem. Soc.* **2009**, *131*, 3796. (c) Roe, D. C.; Marshall, W. J.; Davidson, F.; Soper, P. D.; Grushin, V. V. *Organometallics* **2000**, *19*, 4575. (d) Pilon, M. C.; Grushin, V. V. *Organometallics* **1998**, *17*, 1774. (e) Rh−FHF: Segarra, C.; Mas-Marzá, E.; Lowe, J. P.; Mahon, M. F.; Poulten, R. C.; Whittlesey, M. K. *Organometallics* **2012**, *31*, 8584. (f) Ru−FHF: Jasim, N. A.; Perutz, R. N.; Foxon, S. P.; Walton, P. H. *J. Chem. Soc., Dalton Trans.* **2001**, 1676. (g) Pt−FHF: Jasim, N. A.; Perutz, R. N. *J. Am. Chem. Soc.* **2000**, *122*, 8685. (h) Ni−FHF: Braun, T.; Foxon, S. P.; Perutz, R. N.; Walton, P. H. *Angew. Chem., Int. Ed.* **1999**, *38*, 3326.

(10) Selected examples with copper(II) and nickel(II) as metal ions: (a) Manson, J. L.; Baldwin, A. G.; Scott, B. L.; Bendix, J.; Del Sesto, R. E.; Goddard, P. A.; Kohama, Y.; Tran, H. E.; Ghannadzadeh, S.; Singleton, J.; Lancaster, T.; Möller, J. S.; Blundell, S. J.; Pratt, F. L.; Zapf, V. S.; Kang, J.; Lee, C.; Whangbo, M.-H.; Baines, C. *Inorg. Chem.* **2012**, *51*, 7520. (b) Manson, J. L.; Carreiro, K. E.; Lapidus, S. H.; Stephens, P. W.; Goddard, P. A.; Del Sesto, R. E.; Bendix, J.; Ghannadzadeh, S.; Franke, I.; Singleton, J.; Lancaster, T.; Möller, J. S.; Baker, P. J.; Pratt, F. L.; Blundell, S. J.; Kang, J.; Lee, C.; Whangbo, M.-H. *Dalton Trans.* **2012**, *41*, 7235. (c) Manson, J. L.; Warter, M. L.; Schuelter, J. A.; Lancaster, T.; Steele, A. J.; Blundell, S. J.; Pratt, F. L.; Singleton, J.; McDonald, R. D.; Lee, C.; Whangbo, M.-H.; Plonczak, A. *Angew. Chem., Int. Ed.* **2011**, *50*, 1573.

(11) Levina, V. A.; Rossin, A.; Belkova, N. V.; Chierotti, M. R.; Epstein, L. M.; Filippov, O.; Gobetto, R.; Gonsalvi, L.; Lledós, A.; Shubina, E. S.; Zanobini, F.; Peruzzini, M. *Angew. Chem., Int. Ed.* **2011**, *50*, 1367.

(12) Rossin, A.; Peruzzini, M.; Zanobini, F. *Dalton Trans.* **2011**, *40*, 4447.

(13) (a) Miller, J. M. *Prog. Nucl. Magn. Reson. Spectrosc.* **1996**, *28*, 255. (b) Fernandes, R. G.; Ren, J.; De Camargo, A. S. S.; Hernandes, A. C.; Eckert, H. *J.Phys Chem. C* **2012**, *116*, 6434. (c) Martineau, C.; Fayon, F.; Suchomel, M. R.; Allix, M.; Massiot, D.; Taulelle, F. *Inorg. Chem.* **2011**, *50*, 2654.

(14) (a) Kovács, G.; Rossin, A.; Gonsalvi, L.; Lledós, A.; Peruzzini, M. *Organometallics* **2010**, *29*, 5121. (b) Rossin, A.; Gonsalvi, L.; Phillips, A. D.; Maresca, O.; Lledós, A.; Peruzzini, M. *Organometallics* **2007**, *26*, 3289. (c) Rossin, A.; Kovács, G.; Ujaque, G.; Lledós, A.; Joó, F. *Organometallics* **2006**, *25*, 5010.

(15) Frisch, M. J.; et al. *Gaussian09*, revision A.02; Gaussian Inc.: Wallingford, CT, 2009.

(16) Zhao, Y.; Truhlar, D. G. *Theor. Chem. Acc.* **2008**, *120*, 215.

(17) Zhao, Y.; Truhlar, D. G. *Acc. Chem. Res.* **2008**, *41*, 157.

(18) (a) Andrae, D.; Haeussermann, U.; Dolg, M.; Stoll, H.; Preuss, H. *Theor. Chem. Acc.* **1990**, *77*, 123. (b) Dolg, M.; Wedig, U.; Stoll, H.; Preuss, H. *J. Chem. Phys.* **1987**, *86*, 866.

(19) Dunning, T. H.; Hay, P. J. *Modern Theoretical Chemistry*; Schaefer, H. F., III, Ed.; Plenum: New York, 1976.

(20) Lynch, B. J.; Zhao, Y.; Truhlar, D. G. *J. Phys. Chem. A* **2003**, *107*, 1384.

(21) (a) Höllwarth, A.; Böhme, M.; Dapprich, S.; Ehlers, A. W.; Gobbi, A.; Jonas, V.; Köhler, K. F.; Stegmann, R.; Veldkamp, A.; Frenking, G. *Chem. Phys. Lett.* **1993**, *208*, 237. (b) Ehlers, A. W.; Böhme, M.; Dapprich, S.; Gobbi, A.; Höllwarth, A.; Jonas, V.; Köhler, K. F.; Stegmann, R.; Veldkamp, A.; Frenking, G. *Chem. Phys. Lett.* **1993**, *208*, 111.

(22) Marenich, A. V.; Cramer, C. J.; Truhlar, D. G. *J. Phys. Chem. B* **2009**, *113*, 6378.

(23) The static dielectric constant values of H_2O/THF mixtures at variable composition and at T = 298 K are taken from: Kinart, C. M.; Kinart, W. J. *Pol. J. Chem.* **1994**, *68*, 339.

(24) (a) Gancheff, J. S.; Kremer, C.; Denis, A.; Giorgi, C.; Bianchi, A. *Dalton Trans.* **2009**, 8257. (b) Kovács, G.; Schubert, G.; Joó, F.; Papai, I. *Organometallics* **2005**, *24*, 3059.

(25) Fukui, K. *Acc. Chem. Res.* **1981**, *14*, 363.

(26) The fluoride complex **2** is prepared through a chloride−fluoride exchange from the corresponding chloro complex ($^{t\mathrm{Bu}}$PCP)Ni(Cl) treated with TlF in MeOH (see ref 12). The thallium(I) salt employed is highly hygroscopic; all attempts made to dry it led to its decomposition. Small amounts of water are therefore unavoidable, and they are intrinsic to the preparative procedure employed.

(27) Gakh, Y. G.; Gakh, A. A.; Gronenborn, A. M. *Magn. Reson. Chem.* **2000**, *38*, 551.
(28) Herzfeld, J.; Berger, A. E. *Chem. Phys.* **1980**, *73*, 6021.
(29) The $^{31}P\{^{1}H\}$ NMR chemical shift of the *aquo* species is strongly dependent on the counterion nature; in fact, the corresponding tetrafluoborate complex has δ_P = 69.0 ppm in the same solvent (THF-d_8): see ref 12. Formation of **5** is also confirmed by the appearance of its typical signals on the ^{1}H NMR spectrum. For a more detailed description, see ref 12.
(30) (a) Levina, V. A.; Filippov, O. A.; Gutsul, E. I.; Belkova, N. V.; Epstein, L. M.; Lledós, A.; Shubina, E. S. *J. Am. Chem. Soc.* **2010**, *132*, 11234. (b) Belkova, N. V.; Gutsul, E. I.; Filippov, O. A.; Levina, V. A.; Valayev, D. A.; Epstein, L. M.; Lledós, A.; Shubina, E. S. *J. Am. Chem. Soc.* **2006**, *128*, 3486.
(31) The exact position of the TS for this (rather complex) transformation could not be found because of simultaneous F^- dissociation and water coordination to the nickel(II) center, joint to the hydrogen-bonding network rearrangement that follows HF formation. All attempts made to calculate it failed. Nonetheless, the PES scan along the *d*(Ni−F) reaction coordinate led to a maximum of the energy profile for *d*(Ni−F) = 2.5 Å, which can be reasonably considered to be very close to the real TS geometry. Therefore, the Gibbs energy of this point has been taken as an approximation of the real activation barrier.
(32) Grotthuss, C. J. T. *Ann. Chim.* **1806**, *58*, 54.